Research Article

Erik Förster, Moritz Stürmer, Ulrike Wallrabe, Jan Korvink, Patrick Bohnert and Robert Brunner*

Dual-mode spectral imaging system employing a focus variable lens

DOI 10.1515/aot-2015-0053
Received November 16, 2015; accepted January 8, 2016; previously published online February 4, 2016

Abstract: This paper presents a dual-mode spectral imaging system, which allows switching between pure lateral imaging and the spectrally resolved recording of spatial information. The optical system was equipped with tunable functionalities in order to achieve high flexibility, cover a wide range of object distances, and address extended field angles. A fluidic membrane lens was used for the variable focus, and the recording of the laterally extended scene was made possible by successively adjusting the different tilting angles to the different object positions. The capability and performance of the spectral imaging system were assessed using various test scenes, with different aimed field positions and changing object distances.

Keywords: active or adaptive optics; adaptive imaging; multispectral and hyperspectral imaging; spectrometers and spectroscopic instrumentation.

OCIS codes: (110.1080) active or adaptive optics; (110.1085) adaptive imaging; (110.4234) multispectral and hyperspectral imaging; (120.6200) spectrometers and spectroscopic instrumentation.

***Corresponding author: Robert Brunner,** University of Applied Sciences, Department SciTec, Jena 07745, Germany; and Fraunhofer Institute for Applied Optics and Precision Engineering, Jena 07745, Germany, e-mail: robert.brunner@fh-jena.de
Erik Förster and Patrick Bohnert: University of Applied Sciences, Department SciTec, Jena 07745, Germany
Moritz Stürmer and Ulrike Wallrabe: IMTEK, University of Freiburg, Laboratory for Microactuators, Freiburg 79110, Germany
Jan Korvink: IMTEK, University of Freiburg, Laboratory for Simulation, Freiburg 79110, Germany

1 Introduction

Spectral imaging, or the combined recording of lateral images and spectral information, is a powerful analysis tool for a number of applications, ranging from the agri-food sector [1–3], pharmaceutics [4, 5] and environmental monitoring [6, 7], to biochemistry [8] and military applications [9]. In order to meet the specific requirements of individual applications, many different adapted spectral imaging techniques have been developed over the past few years. Typically, the classification of spectral imaging systems distinguishes between wavelength-scan methods and spatial-scan techniques, such as 'whiskbroom' or 'pushbroom' systems and 'snapshot' methods. In the former systems, a number of two-dimensional images of a scene are acquired at different wavelengths by using discrete or tunable filters, while in the latter, spatial and spectral information can be detected simultaneously in one single step. An overview of the various spectral imaging techniques has been provided in several review articles [10–12].

Owing to the demanding technical challenges for each of these techniques, there is always a trade-off between the different target qualities, like spatial and spectral resolution, and the light collection efficiency and acquisition time. Generally, a single and comprehensive solution for all of the application scenarios seems impossible; yet, the selection of the employed spectral imaging method depends on the specific needs. It is often a compromise with regard to the different optical characteristics, as well as the flexibility and compactness. Once the additional functionalities, such as a variable focus, have been implemented beyond the standard requirements of the spectral imaging system, it becomes increasingly difficult to find an appropriate compromise. In this contribution, we present an alternative approach to the state of the art of a spectral imaging system, with which to overcome the present restrictions. Our setup allowed for dual-mode operation, so that it became possible to switch

between pure lateral imaging and a spectral mode. The imaging mode was based on preceding developments and combined an aspherical hybrid diffractive-refractive lens with a flexible fluidic membrane lens. This combination allowed for the implementation of a light-sensitive optical system with variable focus [13]. In addition, the system compensated for the deterioration of the image quality with an increasing field position by successively addressing different tilting angles using a gimbal mounting. In the first part of this contribution, we present the basic concept and the implementation of our dual-mode system. Afterward, we demonstrated the working principle over a wide range of object distances and for different field positions.

2 Concept of the dual-mode system

The setup concept is depicted schematically in Figure 1 as a superposition of the optical design data and the contours of the involved optical elements for both modes of operation. In consecutive order from the object space (left) to the detector plane (right), the system is comprised of an optical front group, a variable slit aperture, a condenser, a re-imaging group, and finally a 2D-detector-array.

For the lateral imaging, all of the components were oriented in a straight line along the optical axis (see Figure 1A). The optical front group created an intermediate image of the observed scene, while it combined a variable fluid membrane lens and a commercially available aspherical hybrid diffractive-refractive lens. The plano-convex variable lens consisted of a transparent liquid filled cavity with a hard plane inorganic glass substrate at the backend and a flexible optical transparent silicone membrane at the front. The radius of curvature of the silicone membrane could be adjusted by varying the liquid pressure inside the cavity, which was generated by an integrated piezo bending actuator [14, 15]. The variable lens offered a large aperture diameter (7 mm) and appropriate wave-front properties (wave-front error in the range of 0.1 λ–0.2 λ at 633 nm) [16, 17]. The two insets in the upper part of Figure 1A show, schematically, this lens type in the un-actuated and actuated states. The variable focal length of the lens combination allowed the adjustment of the system to different object distances, between 160 mm

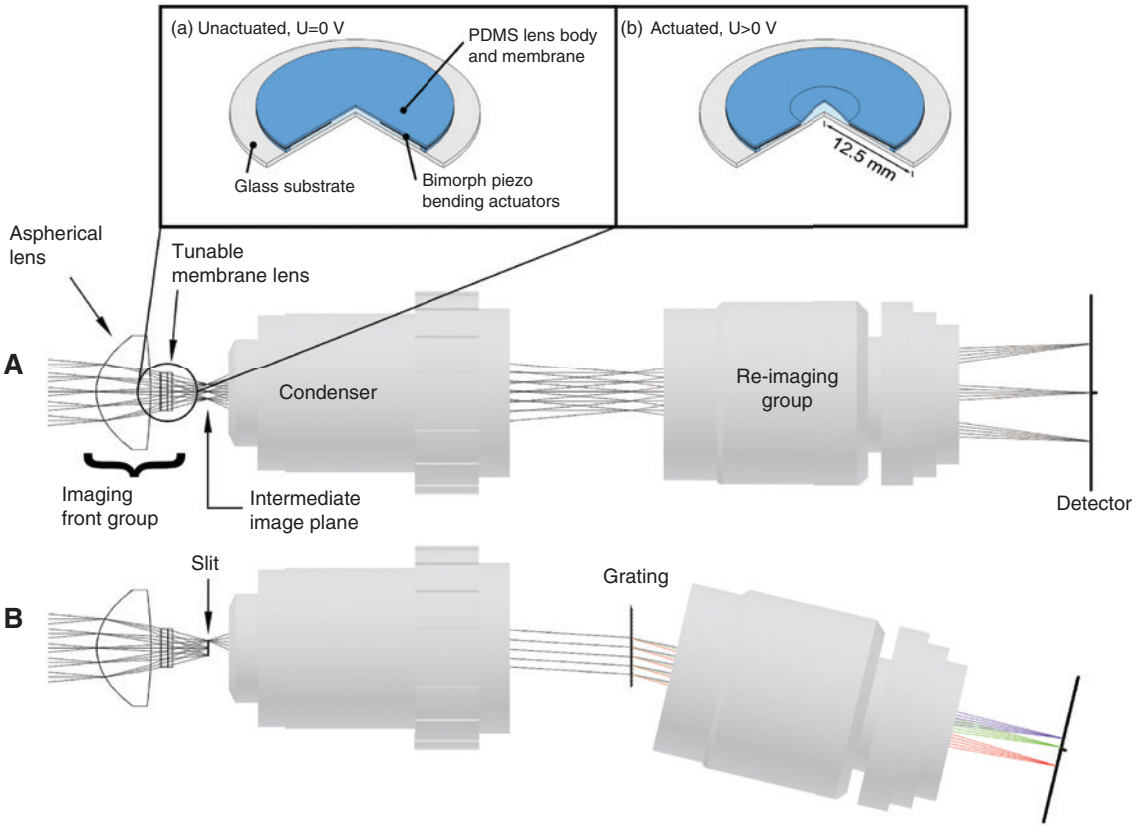

Figure 1: Superposition of the optical design data and contours of the involved optical elements for both operation modes, lateral imaging A and spectral imaging B. The front group encloses a variable fluidic membrane lens, which allows for focal adjustment (actuated and non-actuated states in the upper insets).

and infinity. Based on the fact that the front group only employed two optical elements, its field-dependent resolution was limited. In order to compensate for the associated aberrations, the movement of the front group was enabled by a gimbal-mounted system in which the front group was integrated, so that different field positions could be targeted successively. The working principle and imaging properties of the entire front group and further details about the employed optical components have been discussed extensively [13].

A slit aperture, which was needed for spectral imaging, was located in the intermediate image plane and, in the case of pure lateral imaging, the slit aperture could be opened. The condenser lens (microscope objective, GF Planachromat 12.5×/0.25, Zeiss Jena, Germany) formed a parallel ray bundle from each point of the intermediate image plane, which was re-imaged by the subsequent re-imaging group (Xenoplan 2.8/50-0902, Schneider Kreuznach, Germany) onto the final detector array. From the combined condenser and re-imaging group, a 2.5× magnification could be obtained.

To operate the system in the spectral acquisition mode (see Figure 1B), it was necessary to reduce the gap width of the aperture slit and allow its variable displacement across the intermediate image plane. Depending on the position of the slit, a specific line from the intermediate image plane was selected for spectral decomposition. Furthermore, a diffractive grating was inserted in the beam path between the condenser lens and re-imaging group, with a spatial period of 300 lines/mm, and a blazed-profile designed for a wavelength of 525 nm in the first diffraction order (GT13-03, Thorlabs, USA). For each line selected from the intermediate image plane, the condenser formed a parallel ray bundle, showing a slightly different tilting angle with respect to the optical axis, and therefore, the individual ray bundles hit the dispersive grating at slightly different angles. Behind the grating, the spectrally decomposed parallel rays changed the direction of propagation, which was dependent on both the wavelength and the incidence angle. This means that the final optical group, together with the detector, had to be rotated to compensate for the direction change induced by the diffraction grating, and the center of this rotation was located on the surface of the dispersive grating. The final optical group created an image of each line selected from the intermediate image plane on the detector. One direction of the detector corresponded to the lateral slice selected by the slit aperture, whereas the spectral information was stretched in a perpendicular direction. For a detector array, we used a monochrome CCD-sensor (DMK 23U274, The Imaging Source, Germany). Finally, for a simple colored representation in the lateral imaging mode, we exchanged the monochrome camera with an analog color model (DFK 23U274, The Imaging Source, Germany).

3 Experimental verification

After the implementation of the dual-mode system, the basic features of both the pure lateral imaging mode and the spectral acquisition mode were evaluated. In addition to the basic operation modes, the system's tunable functionality was tested, which allowed for addressing a wide range of different object distances and the recording of a laterally extended object field. For these purposes, the tunable lens and the rotational movement of the system's front group were applied.

In these experiments, light-emitting sources were used as test objects, in which each of them having a specific spectral fingerprint. To test various application scenarios, the light sources were arranged in different configurations in the object space, and for each of the evaluated configurations, both the lateral positions of the light sources as well as their distances to the imaging system were reorganized. A main test target object was prepared for the qualitative and quantitative validation of the spectral imaging system. The square front panel of this test target was 25 cm×25 cm and was comprised of several specific light sources. Each light source emitted a characteristic spectrum, which was previously calibrated. While some of these light sources possess a continuously distributed spectrum, others only emit specific wavelengths. A diffuser disc in front of each light source was used for uniform and almost homogeneously emitted light distribution. Typically, the distance between the test target and spectral imaging system was between 1.5 m and 2.5 m.

For the pure lateral imaging mode, we employed a color sensor that allowed the simple representation of the observed scene in terms of the three basic colors. In the spectral imaging, we used optionally both sensor types, the color and monochrome cameras. The color camera offered a vivid illustration and qualitative view of the spectral distribution for each point of the selected line from the object space. Moreover, the displayed color gradient correlated directly with the detected wavelength. For a quantitative analysis of the spectra, we used the monochrome camera, and from the readout signal, the associated incoming light intensity was derived as a function of the wavelength. Here, it was essential to take the wavelength-dependent sensitivity of the camera into account. We calibrated the detector beforehand, by using the wavelength-dependent correction function provided

by the camera manufacturer. In this way, it was possible to carry out a quantitative spectral measurement for each selected spatial position.

4 Laterally distributed objects located at the same distance

The upper line of Figure 2 shows a lateral image and a magnified section of the test target recorded with the color camera in the pure imaging mode. In this case, the object distance was 2.5 m, so that the main test objects covered a field angle of ±2.8°. All of the sources in the test target were switched on and emitted in their characteristic colors. The specific sources were arranged in mirror symmetry across the test target, so that the same color arrangement was visible on the left and on the right. Similar to the human eye, the color camera offered only a qualitative color impression and rough differentiation between blue, yellow, red, and white. In order to obtain detailed data about the spectral content of the particular light sources, we switched to the spectral image mode in which the aperture slit was narrowed, the dispersion grating was turret shifted, and the final camera lens combined with the detector was rotated to the appropriate angle. The selection of a specific object line was achieved by shifting the aperture slit to the desired position in the intermediate image field.

In the lower part of Figure 2, the wavelength-dependent emitted intensity has been displayed for four different selected object lines that correspond to the white lines indicated in the lateral image of Figure 2, marked as M, 1, 2, and 3. In order to visualize the wavelength dependency, these images were also captured with the color camera. For the subsequent quantitative measurements, the

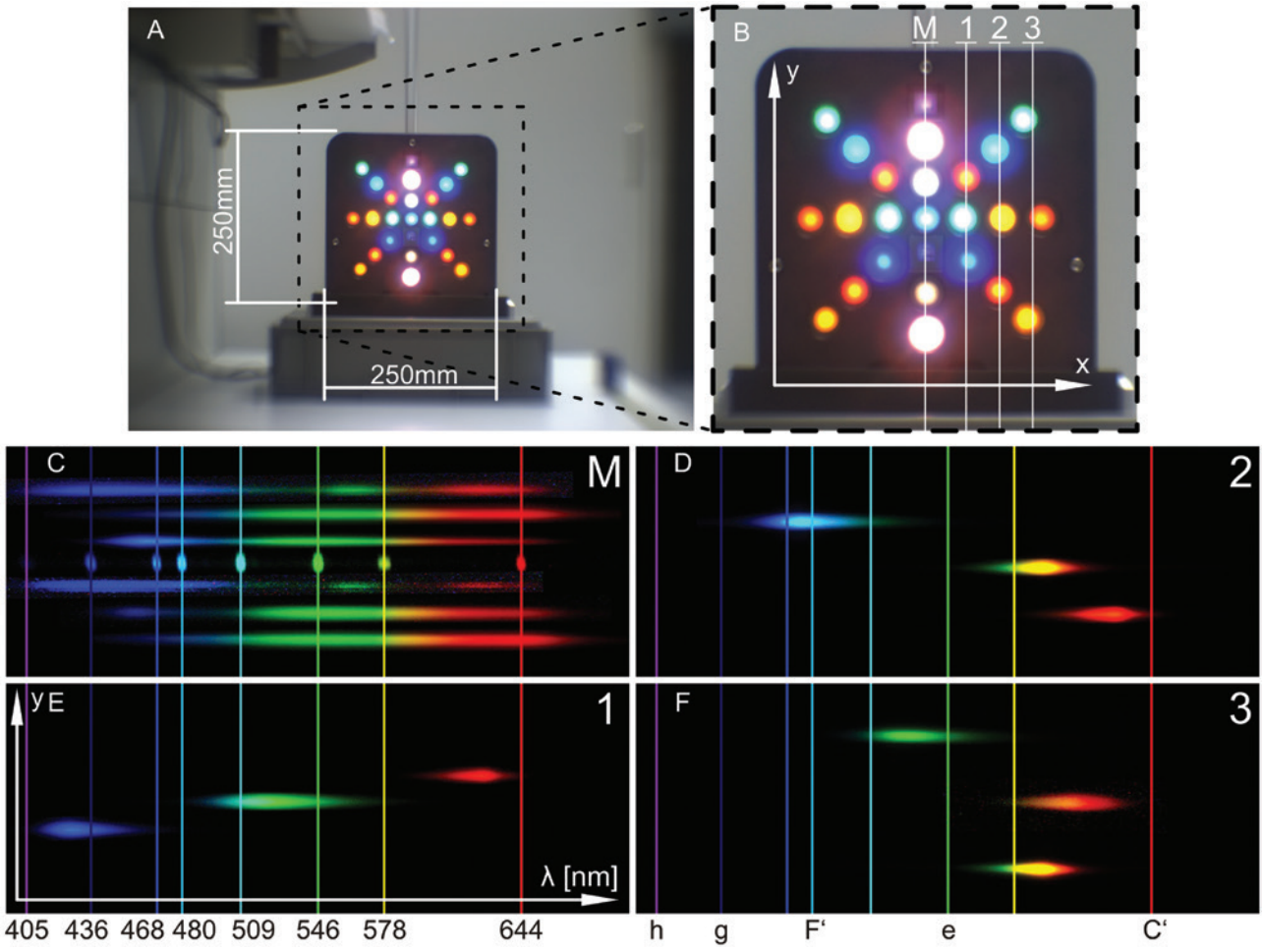

Figure 2: Laterally distributed objects (light sources) located at the same distance (2.5 m). (A and B) in the upper line show a lateral image of the main test object and a magnified view. (C–F) display the spectral representation for four selected lines (positions marked M, 1, 2, and 3 in Figure 4B).

monochrome camera was employed; and for each of the four images, the vertical axis corresponded to the lateral position of the selected object line, while the horizontal axis depicted the observed wavelength.

Figure 3 shows the spectral representation of line 'M', as well as the individual spectra of each comprising light source, as the normalized intensity dependent on the wavelength. An HgCd-lamp was placed at the central position of the spectral representation of line 'M'; its spectrum was discrete, with characteristic intensity peaks. These characteristic lines were used as reference points for the spectral distribution of the other light sources and are indicated in all four spectral images in Figure 2, which are related to the selected lines (M, 1, 2, and 3).

The uppermost spectrum of line 'M' (Figure 3, top) belonged to an RGB-LED, in which red, green, and blue LEDs are emitted simultaneously, resulting in a combined 'white-light'-emitting light source. The measured spectrum showed three separate intensity maxima, which can be attributed to the three LEDs. However, the second spectrum was formed by a classical light bulb, showing a continuous spectrum with a maximum in the longer wavelength region. The next continuous spectrum, just above the spectrum of the HgCd-lamp, belonged to a phosphor-converted white LED. An RGB-LED was located directly below the HgCd-lamp and was identical to the one at the top (with the exception of the addition of a neutral density (ND) filter), so that the spectrum appeared much weaker. At the second-to-last position, an additional phosphor-converted white LED was located. Contrarily to the first LED, a different conversion phosphor was employed, thus, revealing a slightly red-shifted spectrum. At the bottom position, a second classical light bulb (albeit much brighter than the first) was integrated into the test target. By moving the slit from the center of the intermediate image plane to the right, the line positions marked 1–3 in Figure 2 were selected successively. The corresponding spectra for each of these lines are also displayed in Figure 2.

5 Test objects distributed across the observed field and located at different distances

In the following object scene, the light-emitting test elements showed varying distances from the spectral imaging system, on the one hand, while on the other, they were distributed across the observed lateral field. The main test

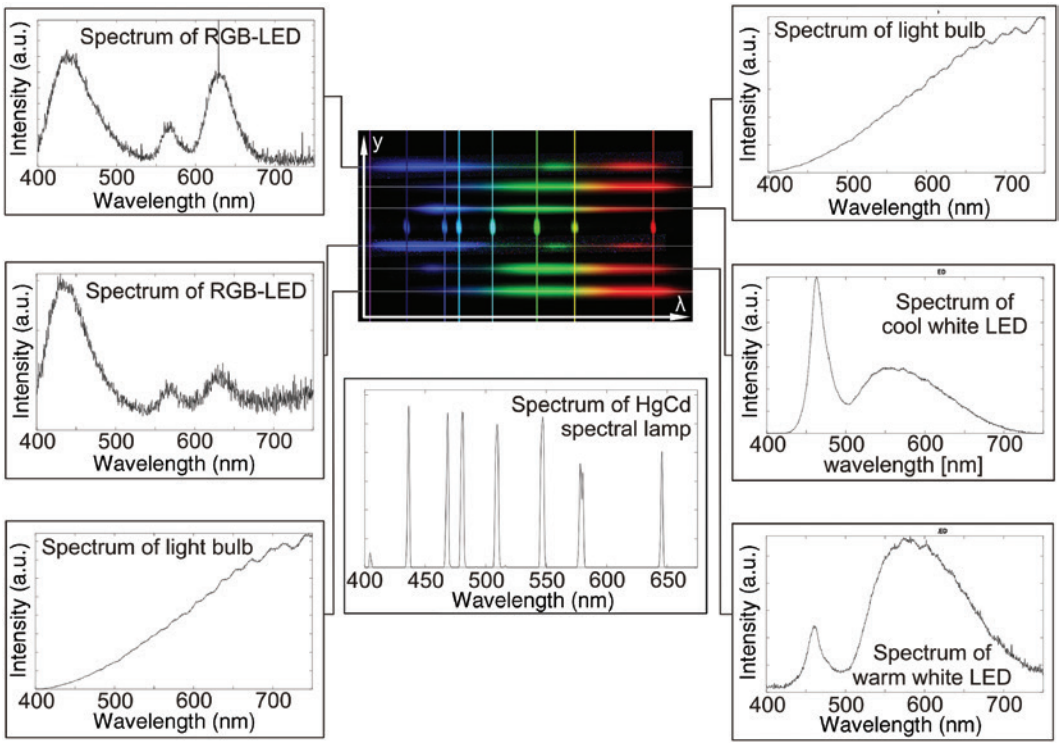

Figure 3: Spectral representation of the selected center line from position M in Figure 2 combined with measured normalized spectra of the seven individual light sources.

object was placed in the background at a distance of 2.5 m, and two additional light sources were fixed to the main target, one at the upper right corner and the second at the upper left. The third light source, which was mounted on a separate post, was displaced at the center of the scene at an intermediate object distance. In addition, a white light LED was placed in the foreground next to the spectral imaging system. The left column of Figure 4 displays the recorded lateral images, with the focus adjusted to the different object distances. The vertical white stripe in each of the lateral images indicates the selected slit position for the accompanied spectral line representation, which is depicted in the second column of Figure 4.

In the two upper lateral images, the focus was set to a further distance targeting the main test object. The first row of Figure 4 represents a slit position in which two light sources were simultaneously detected. The upper light source was fixed to the main test object and, therefore, also in focus, so that a small-sized emitting area was observable. The second lower source was located at a nearer distance and, due to the mismatch of the adjusted focus and object distance, appears to be blurred in the

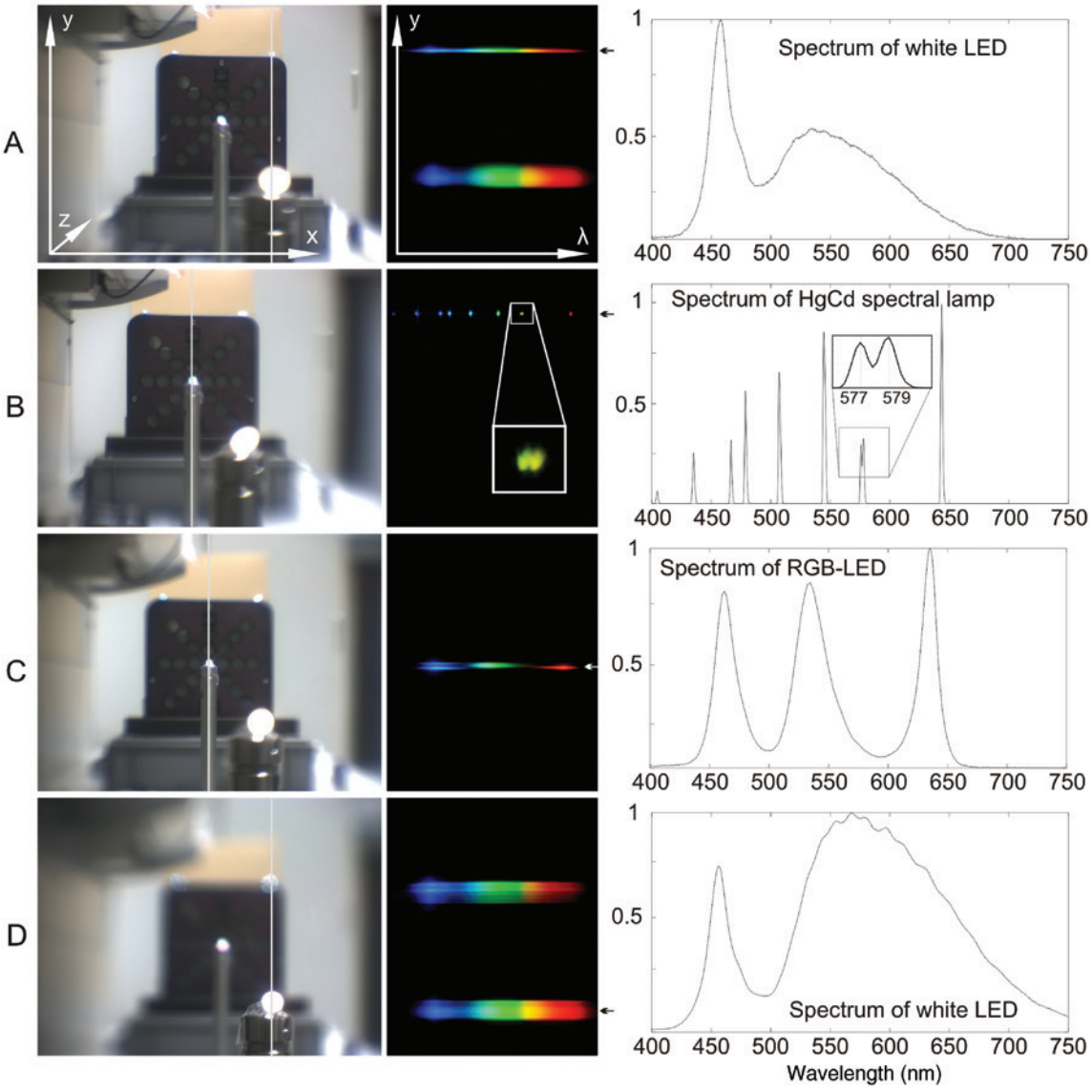

Figure 4: Test objects distributed across the observed field and located at different distances. The left row shows lateral images with adjusted focus to (A) and (B), the intermediate range (C), and the near distance (D). The white line in each of the lateral images indicates the selected slit position. Center row: Corresponding spectral representations. Right row: Spectra of specific sources. In the inset of the HgCd spectrum, the two separated orange lines (577.0 nm and at 579.1 nm) are depicted.

lateral image. Owing to the adjusted focus position, the spectrum belonging to the upper light source appears sharp in the vertical direction, while the spectrum of the lower source is rather broad along the slit orientation.

The result of the quantitative measurement of the emitted intensities as a function of the wavelength is displayed in the following diagram (on the right). The monochrome camera was employed for this quantitative measurement. Overall, the spectrum showed a distinct peak in the blue wavelength region and a broad, continuous wavelength distribution with a broad maximum in the green wavelength range. Because of the particular focus setting, and the spectrum of the upper light, the source appears vertically sharp and concentrated. For the spectral representation displayed in the second row of Figure 4, the slit picked the object line, which included the light source on the upper left corner of the test target. This source was the emitting end of a glass fiber in which the light of an HgCd-lamp was coupled, so that the related spectrum showed the characteristic line spectrum.

A closer and more quantitative examination of the spectrum allowed us to clearly distinguish between the two directly adjacent lines in the orange wavelength range. These lines, at 577.0 nm and at 579.1 nm, belonged to the characteristic Hg spectrum (see also the inset and magnified section of the spectrum). It follows that the spectral resolution of the spectral image sensor was explicitly better than 2 nm, when the two lines were separated.

The spectral resolution of the system is dependent on the width of the line-selecting slit. Explicitly, the slit diameter corresponds to a residual divergence of the ray bundle leaving the condenser optics. Owing to this residual divergence, the diffraction grating is illuminated by angle distribution, which finally leads to a blurring of the image in the detector plane for a specific wavelength. Additionally, also the numerical aperture of the final reimaging group influences the spectral resolution of the system. It is sufficient to select a numerical aperture, which allows that the diffraction-limited spot size is in the range of the pixel dimension of the detector. The demonstrated spectral resolution of approximately 2 nm is comparable to the performance of commercial spectrometers, which are typically used for biomedical applications, for process control in the glass industry or in the pharmaceutical production (e.g. spectrometer from company 'ZEISS': CGS UV/NIR).

In the third row, the focus was adjusted to the intermediate image distance, so that the central light source on its post was clearly resolved. However, the light sources in both the background and foreground appeared blurred. Moreover, the spectral representation of the chosen slit position showed a three-part structure, with maxima in the blue, green, and red spectral ranges. The cross section of the spectrum showed that the different maxima were emitted with the same intensity. Finally, the foreground was brought into focus so that the upper right light source appeared to be well resolved (lowest line of Figure 4). In this position, the slit again covered both sources on the right, which is similar to the situation shown in the first line, but this time, the focus adjustment was reversed.

6 Spectral imaging of a laterally extended scene

Commonly, the induced aberrations of an optical system increase with an enlarging field position, so that the imaging quality in the outer regions of the systems is reduced when compared to the central area. Our system tended to be prone to aberrations, such as coma, which were intensified by increasing the object field. In order to compensate for the aberrations in the large field angles, our optical system allowed for the successive targeting of decisive field positions and the capture of lateral and spectral information from the different directions. Here, the optical front group was redirected by a gimbal-mounted system [13].

To test the characteristics of our spectral sensor, we modified the test scene so that a larger field angle could be observed. For this, the distance from the test object to the spectral imaging system was simply reduced to 1.5 m. In this scenario, the angle distance between the distant light sources, which were integrated in the test object, was larger. In addition, two white marks were attached to the upper left and lower right edges of the dark test object. To pronounce the contours of the respective light sources in the direct vicinity of the white corner angles, both were partially covered with two small stripes.

In the upper row of Figure 5, two lateral images of the test object are depicted. In Figure 5A, the optical system was oriented by the gimbal-mounted system toward the upper left corner of the test object. In this image, both the white corner angle and the two-stripe structured light source are clearly resolved. In contrast, and as expected, the light source and structures near the lower right corner appear to be significantly blurred, due to the aberrations related to the large field position. Figure 5B shows the reverse situation. Here, the optical front group was turned by the gimbal mounting to point in the direction of the lower right corner of the test target, which now appears highly resolved, whereas the upper left region of the test target is disrupted by aberrations.

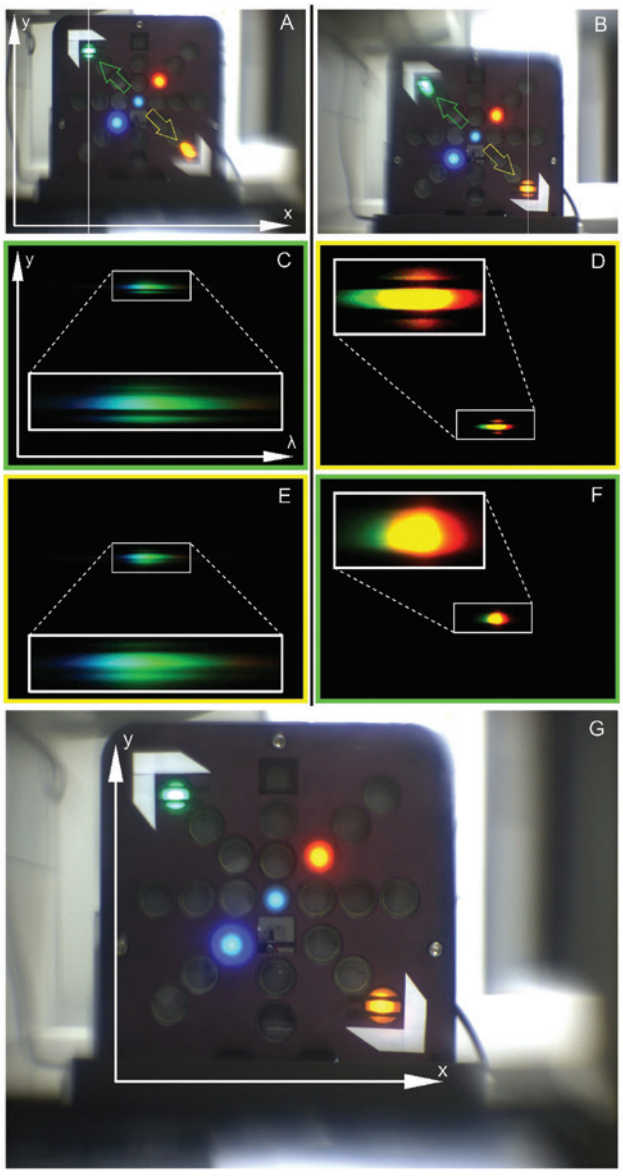

Figure 5: Spectral imaging of a laterally extended scene by successively redirecting the optical system. For the lateral images of the upper line, the system was oriented to different field positions (left upper corner and right lower corner of the test target). (C–F) Spectral representations of selected slit positions for both orientation directions. Bottom (G) Composite image in which the highly resolved regions from each sub-image (A and B) were combined.

The central part of Figure 5 depicts the related spectral line representations for the different cases. In this case, the slit in the intermediate image plane was oriented vertically and parallel to the edges of the test object. For better visualization, the settings of the slit positions are indicated by the white vertical lines in Figure 5A and B. Moreover, the spectral line representations shown in Figure 5C and E have been recorded with the slit alignment intersecting the position of the upper left light source. In contrast to Figure 5D and F, the slit was moved to the right of the observed scene, so that the lower right light source was included. A further distinction between the different spectral line representations concerns the particular target area in the observed scene. For the spectra shown in Figure 5C and F, the optical system was oriented to the upper left corner of the test object, whereas in Figure 5D and E, the system pointed to the lower right corner. The outer frame of each single image, represented in Figure 5C through F, indicates the complete spectral line representation for the different cases. For a better recognition of the essential spectral details in each sub-image, the relevant parts were additionally displayed in a magnified view as an inset in the respective line representation. In Figure 5C, the blue-green spectrum of the upper left light source is clearly observable in the horizontal direction; while along the vertical axis, the lateral two-stripe decorated light source is well resolved. When the optical system was pointed in the direction of the lower right corner, the spectrum of the upper left source was still recognizable, but its lateral information (two-stripe profile) was reduced (Figure 5E). Figure 5D and F show the analogous results for addressing the lower left light source.

Following the capture of the individual lateral images of the scene (Figure 5A and B), a final overall image could be processed. With the aid of an imaging processing software, the highly resolved regions from both sub-images were selected and, subsequently, combined to form the resulting final overall image. Figure 5G shows the result of this process in a clearly resolved image, which is clearly resolved into its very edges.

7 Conclusion

Here, we have introduced a dual-mode imaging system, which can be operated in a mode for pure lateral imaging as well as a mode for spectral detection. The optical system was equipped with tunable and moveable functionalities in order to obtain high flexibility and to cover a wide range of object distances, as well as to address extended field angles. In particular, a flexible fluidic membrane lens was used for the variable focus. Tunable and moveable functionalities were also applied for the spectral imaging mode. In this study, the spectral information was captured in lines by guiding a slit selectively across the intermediate image of the observed scene. The demonstrated spectral resolution of 2 nm is appropriate for a broad application range, comprising biomedical applications and also process control for industrial production. In principle, an

improved spectral resolution is achievable by changing the slit width and adapting the final re-imaging group.

In the implementation presented, the employed tunable and moveable components were operated mechanically and/or controlled externally. However, there was no principle limitation to extend the setup to an automatically controlled spectral imaging system, which could capture the full spectral information from an extended field of view and for different object distances. A tunable slit aperture, which could be adjusted to different positions by an integrated electrowetting actuation, has already been presented [18]. The integration of such a device into the spectral imaging system could allow for further compactness.

Acknowledgments: We are greatly indebted to Jonas Alteneder, who supported the processing of the individual sub-images. This work was funded by the German Research Foundation DFG within the Priority Program 'Active Micro-optics', under the project EAGLE-II, and by the BMBF in the FhG-project using the acronym 'MIRO'.

References

[1] A. A. Gowen, C. P. O'Donnell, P. J. Cullen, G. Downey and J. M. Frias, Trends Food Sc. Technol. 18, 590–598 (2007).
[2] C. B. Singh, D. S. Jayas, J. Paliwal and N. D. G. White, Proc. SPIE 7676, 767603 (2010).
[3] Q. Ran, W. Li, Q. Du and C. Yang, J. Appl. Remote Sens. 9, 097298 (2015).
[4] S. J. Hamilton and R. A. Lodder, Proc. SPIE 4626, 136 (2002).
[5] Y. Roggo, A. Edmond, P. Chalus and M. Ulmschneider, Anal. Chim. Acta 535, 1–17 (2004).
[6] M. Moroni, E. Lupo, E. Marra and A. Cenedese, Procedia Environ. Sci. 19, 885–894 (2013).
[7] A. M. Melesse, Q. Weng, P. S. Thenkabail and G. B. Senay, Sensors 7, 3209–3241 (2007).
[8] R. A. Schultz, T. Nielsen, J. R. Zavaleta, R. Ruch, R. Wyatt and H. R. Garner, Cytometry 43, 239–247 (2001).
[9] X. Briottet, Y. Boucher, A. Dimmeler, A. Malaplate, A. Cini, et al., Proc. SPIE 6239, 62390B-1 (2006).
[10] Y. Garini, I. T. Young and G. McNamara, Cytometry Part A 69A, 735–747 (2006).
[11] Q. Li, X. He, Y. Wang, H. Liu, D. Xu and F. Guo, J. Biomed. Opt. 18, 100901-1–100901-28 (2013).
[12] N. Hagen and M. W. Kudenov, Opt. Eng. 52, 090901-1–090901-23 (2013).
[13] E. Förster, M. Stürmer, U. Wallrabe, J. Korvink and R. Brunner, Opt. Express 23, 929–942 (2015).
[14] J. Draheim, F. Schneider, R. Kamberger, C. Mueller and U. Wallrabe, J. Micromech. Microeng. 19, 095013 (2009).
[15] J. Draheim, T. Burger, F. Schneider and U. Wallrabe, in 'Proceedings of IEEE Conference on MEMS 2011 (IEEE 2011) ', pp. 692–695.
[16] F. Schneider, J. Draheim, R. Kamberger, P. Waibel and U. Wallrabe, Opt. Express 17, 11813–11821 (2009).
[17] J. Draheim, F. Schneider, T. Burger, R. Kamberger and U. Wallrabe, 'in '2010 International Conference on Optical MEMS and Nanophotonics', (2010), pp. 15–16.
[18] S. Schuhladen, K. Banerjee, M. Stürmer, P. Müller, U. Wallrabe, et al., Light Sci. Appl. 5, e16005 (2016).

Erik Förster
University of Applied Sciences, Department SciTec, Jena 07745, Germany

Erik Förster studied physical technology and laser- and optotechnology at the University of Applied Sciences Jena. He worked for several years at the Fraunhofer IOF Jena, department of microoptics, on the development of optical instruments for industrial applications. Currently he is PhD student at the University of Applied Sciences Jena, with focus on spectroscopy and hyperspectral imaging.

Moritz Stürmer
IMTEK, University of Freiburg, Laboratory for Microactuators, Freiburg 79110, Germany

Moritz Stürmer is a PhD student at the IMTEK Laboratory for Microactuators at the University of Freiburg. His research focusses on adaptive optical components with integrated actuation, especially tunable lenses and switchable diffraction gratings.

Ulrike Wallrabe
IMTEK, University of Freiburg, Laboratory for Microactuators, Freiburg 79110, Germany

Ulrike Wallrabe studied physics at Karlsruhe University, Germany. In 1992 she received her PhD degree for mechanical engineering of microturbines and micromotors. From 1989 to 2003 she was with the Institute for Microstructure Technology at Forschungszentrum Karlsruhe (today KIT) working on microactuators and Optical MEMS. She holds a Professorship for Microactuators at the Department of Microsystems Engineering, IMTEK, at the University of Freiburg, Germany, since 2003. Her work focus lies in magnetic

microstructures including processes for magnetic materials and micro coils and in adaptive optics, using piezo actuators to tune elastic lenses and mirrors. In the year 2010 she was granted an internal fellowship at the Freiburg Institute of Advanced Studies, FRIAS. Since 2012 she is a member of the Cluster of Excellence BrainLinks-BrainTools.

Jan Korvink
IMTEK, University of Freiburg, Laboratory for Simulation, Freiburg 79110, Germany

Jan G. Korvink is currently Professor and executive director of the Institute of Microstructure Technology at Karlsruhe Institute of Technology. His research interests cover the development of ultra low cost micromanufacturing methods, microsystem applications in the area of magnetic resonance imaging, and the design and simulation of micro and nano systems. He is author or co-author of more than 300 technical publications in the broad area of microsystems. Dr. Korvink is a member of IEEE, the ASME, and a Fellow of the Royal Society of Chemistry.

Patrick Bohnert
University of Applied Sciences, Department SciTec, Jena 07745, Germany

Patrick Bohnert studied precision engineering and scientific instrumentation at the University of Applied Sciences Jena. Now he works as CAD designer and FEM specialist at the research group of Prof. Brunner.

Robert Brunner
University of Applied Sciences, Department SciTec, Jena 07745, Germany; and Fraunhofer Institute for Applied Optics and Precision Engineering, Jena 07745, Germany
robert.brunner@fh-jena.de

Robert Brunner received his PhD degree in the field of near-field optical microscopy from the University of Ulm/Germany. Following a postdoc visit at the Universityof Illinois, Urbana-Champaign, he worked for 12 years in the Research& Technology Center of the Carl-Zeiss company in Jena,Germany. Between 2001 and 2009 he was the responsible Lab Manager for the Microstructured Optics Group. Since 2010 he is Professor for Applied Optics at the University of Applied Sciences in Jena. His current research interests are hybrid diffractive/refractive optics, subwavelength structures, refractive micro-optics, interference lithography and bio-inspired optics.